Stented valve dynamic behavior induced by polyester fiber leaflet material in transcatheter aortic valve devices

Hoda Hatoum, MS[1], **Frederick Heim, PhD**[2], and **Lakshmi Prasad Dasi, PhD**[1]

[1]Department of Biomedical Engineering, the Ohio State University, Columbus, OH, United States

[2]Laboratoire de Physique et Mécanique Textiles, Mulhouse, France

Abstract

Objective—This study aims at assessing the global dynamic behavior, elastic deformability, closing energy and turbulence of rigid versus deformable stented (RS vs DS) valve systems with deformable and rigid textile materials (DT vs RT) through studying the stent-valve interaction compared to a bioprosthetic material in transcatheter aortic valves (TAV).

Methods—Three 19mm stented textile TAV designs (RS-DT, RS-RT and DS-RT) with different stent and leaflet properties were tested and compared with a control bioprosthetic TAV (RS-DB) in a left heart simulator flow loop under physiological pressure and flow. Particle Image Velocimetry and high speed imaging were performed. Pressure gradients (PG), leakage fractions (LF), Pinwheeling indices (PI), closing energy (E) and Reynolds shear stresses (RSS) were calculated.

Results—(a) PGs and LFs were 11.86±0.51mmHg, 11.70±0.34%; 8.84±0.40mmHg, 29.80±0.76%; 11.59±0.12mmHg, 14.23±1.64%; and 7.05±0.09mmHg, 12.08±0.45% % for RS-DB, RS-DT, RS-RT and DS-RT respectively. (b) PIs were 15.79±2.34%, 4.36±0.84%, 2.47±0.51% and 2.03±0.33% for RS-DB, RS-DT, RS-RT and DS-RT respectively. (c) E is lowest for DS-RT (0.0010±0.0002J) followed by RS-RT (0.0017±0.0002J), RS-DB (0.0023±0.0004J) and highest with RS-DT (0.0036±0.0007J). (d) At peak systole lowest RSS was obtained with RS-DT (87.82±0.58Pa) and highest with DS-RT (122.98±1.87Pa).
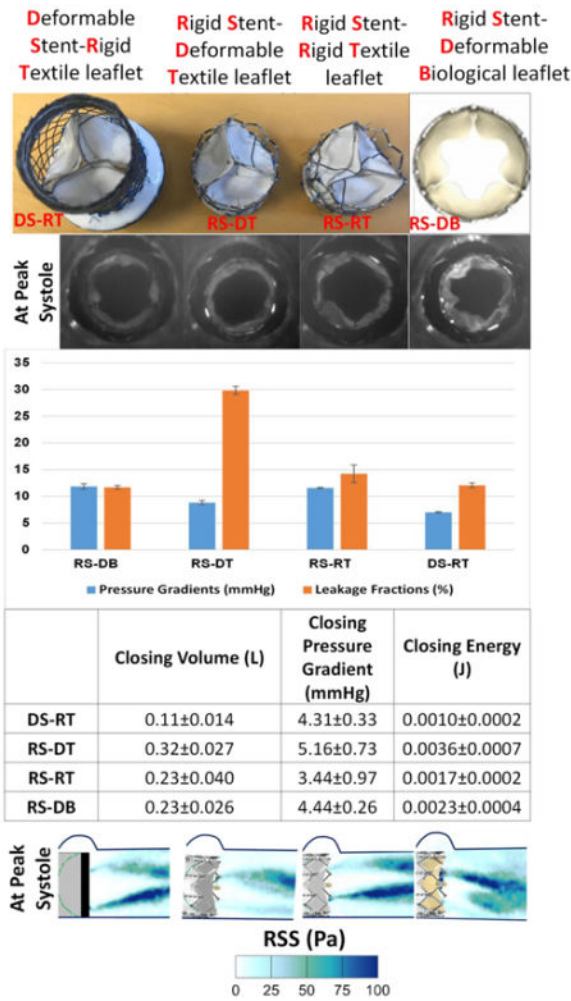
Conclusion—PGs, LFs, PIs and E were improved with DS-RT compared to other textile TAVs and RS-DB. Despite achieving more RSS than the rest of TAVs, DS-RT still falls within the same range of RSS produced by the other 2 valves and control exceeding the threshold for platelet activation.

Graphical Abstract

Address for correspondence and reprints: Lakshmi Prasad Dasi, PhD, Associate Professor, Department of Biomedical Engineering, The Ohio State University, 473 W 12th Ave., Columbus, OH 43210, TEL: (614) 247-8313, lakshmi.dasi@osumc.edu.

Deformable Stent-Rigid Textile leaflet — DS-RT
Rigid Stent-Deformable Textile leaflet — RS-DT
Rigid Stent-Rigid Textile leaflet — RS-RT
Rigid Stent-Deformable Biological leaflet — RS-DB

At Peak Systole

Pressure Gradients (mmHg) / Leakage Fractions (%)
RS-DB, RS-DT, RS-RT, DS-RT

	Closing Volume (L)	Closing Pressure Gradient (mmHg)	Closing Energy (J)
DS-RT	0.11±0.014	4.31±0.33	0.0010±0.0002
RS-DT	0.32±0.027	5.16±0.73	0.0036±0.0007
RS-RT	0.23±0.040	3.44±0.97	0.0017±0.0002
RS-DB	0.23±0.026	4.44±0.26	0.0023±0.0004

At Peak Systole

RSS (Pa)
0 25 50 75 100

Keywords

Transcatheter aortic valves; textile valves; bioprosthetic valves; turbulence; deformability

Introduction

Transcatheter aortic valve (TAV) replacement (TAVR) emerged as a percutaneous alternative procedure for surgical aortic valve replacement procedures especially for high-risk patients[27, 30]. TAVs consist of a compressible stent associated with flexible biological tissue material[2], prone to degradation once associated with stent material[18], and leading to possible valve failure. Generally, if the valve leaflet is too rigid, larger radial forces will be applied on the stent at the level of the leaflet-stent fixation points. Consequently, the stent will deform if it is flexible enough, or the fixation points will transmit heavier load if the stent is more rigid. An exaggerated deformation of the stent could jeopardize the anchoring, and the stent could migrate, while exaggerated load on the fixation points could lead to material rupture. In recent studies, Heim et al. showed that woven polyester textile, already largely used in grafting, could become a potential candidate to replace degenerated human valve[33, 34].

Textile is less deformable than biological tissue and the flexibility of the valve tissue plays a major role in the stress which is transferred to the stent and to the vessel wall over the valve closing cycle[2, 32]. Textile woven material is less flexible than biological tissue. Hence, it is important to study the stent valve interaction in order to assess the global dynamic behavior and elastic deformability of the stented valve system when textile material is used.

In addition to the way TAV stent and leaflet interact, the relatively rapid degeneration of TAVs compromise their durability due to the mechanical forces exerted on the leaflets as they interact with the pulsatile blood flow and lead to having the patient go through another probable implant[2, 3, 35]. Turbulence distal to heart valves during forward flow is the fundamental fluid dynamics phenomenon responsible for pressure gradient as well as hemolysis and platelet activation[16]. Specifically turbulence occurs when the velocity is high enough that viscosity is unable to diffuse and damp any local fluctuations in velocity leading to an exponential rise of spatial and temporal fluctuations in velocity. These turbulent fluctuations in velocity lead to significantly strong shear stresses that blood cells and platelets experience compared to laminar flows[4, 24, 37] and is dependent on the valve geometry (smoothness of inflow, stent elements etc.), leaflet performance (such as flutter), and distal diameter of the aorta relative to the valve orifice area. These turbulent stresses are referred to as Reynolds stresses and have been well known to correlate with hemolysis and platelet activation. Non-physiological turbulent flow after valve implantation was associated with blood damage ranging from platelet activation (to probably thrombosis) and hemolysis[7, 10, 26, 31].

The objective of this study is (1) to assess the global dynamic behavior and elastic deformability of the stented valve system when textile material is used through studying the stent-valve interaction compared to a bioprosthetic material and (2) to assess the different hemodynamic performances of the TAVs and the turbulence engendered at their outflows as a function of the various stent-valve interactions.

Methods

Valve material and stent selection and deployment

Three stented valve designs (Fig. 1) of 19mm internal diameter were tested as follows:

1. Rigid Stent (RS) with a Deformable Textile (DT) heart valve (Fig. 1a). In this RS-DT design, the woven fabric yarns (warp and weft) are inclined, oriented diagonally to the valve axis whereas one of their extremities is free to move at the valve free edge level. Once the leaflet is under pressure, both yarn directions are able to stretch making the leaflet deformable.

2. Rigid Stent (RS) that is commercially available and laser-cut with a Rigid Textile (RT) heart valve (Fig. 1b). In this RS-RT design the woven fabric yarns (warp and weft) are oriented respectively in the valve axis and circumferential directions. Once the leaflet is closed under pressure, the circumferential yarns, fixed at both extremities to the stent, are able to stretch only in a limited way. This limits the deformation of the leaflet.

3. Deformable Stent (DS) with a Rigid Textile (RT) heart valve (Fig. 1c). In this design, the fabric is oriented in a straight way with respect to the axis of the stent but the stent is made from braided wire rather than being laser cut, which makes it more flexible.

Details of the textile materials are provided in Table 1. The radial stiffness is respectively 160N/mm for the laser cut stent and 25N/mm for the braided one. These devices were compared to a control system. A rigid stent with a deformable biological (RS-DB) heart valve was used as control. The RS-DB stent is a commercially available laser-cut stent.

Figure 2 elucidates the behavioral difference between the textile material described above (RT and DT). If a woven fabric is extended either along the yarn orientation or at 45° angle, different mechanical behaviors can be observed as presented in Figure 2. Actually the deformation of the fibrous construction depends on the orientation of the elementary fabric mesh unit with respect to the extension force. The elementary unit is the zone delimited by 2 weft and 2 warp yarns (grey zones in the figure). The following cases can be considered:

a. The load is along the yarns orientation: the elementary unit deforms only slightly because the surrounding yarns, which are only slightly crimped at the beginning become straight rapidly and withstand the load. The fabric is only poorly deformable.

b. The load is at 45°: the diamond shape of the elementary unit deforms as the yarns tend to align in the load direction. The fabric is much more deformable.

To evaluate post-TAVR hemodynamics and turbulence, measurements described below were conducted on the 4 TAVs implanted in an aortic valve chamber.

Hemodynamic assessment

Hemodynamic parameters were evaluated in a pulsatile left heart simulator under physiological flow and pressure as previously described [14, 15] at a cardiac output of 3L/min. The working fluid in this study was a blood analogue mixture of water-glycerine (99% pure glycerin) producing a density of 1060Kg/m^3 and a kinematic viscosity of 3.5cSt. 100 consecutive cardiac cycles of aortic pressure, ventricular pressure and flow rate data were recorded at a sampling rate of 100Hz. The mean transvalvular pressure gradient (PG) is defined as the average of positive pressure difference between the ventricular and aortic pressure curves during forward flow. Average leakage fractions (LF) represent the ratio of leakage volume (LV), to the total forward flow volume (FV) as follows:

$$LF = \frac{LV}{FV} \quad (1)$$

The effective orifice area (EOA) is an important parameter to evaluate valve orifice opening. EOA was computed using the Gorlin's equation:

$$EOA = \frac{Q}{51.6\sqrt{PG}} \quad (2)$$

Where Q represents the root mean square aortic valve flow over the same averaging interval of the PG. The pinwheeling index (PI) is an indicator with implications on leaflet durability and resilience[5, 9, 23]. It is computed from still frames obtained from high-speed imaging as follows and in accordance with Hatoum et al[16]:

$$PI = \frac{L_{actual} - L_{ideal}}{L_{ideal}} \quad (3)$$

Where L_{actual} represents the deflected free edge of the leaflet and L_{ideal} represents the unconstrained ideal configuration of the leaflet free edge.

Two parameters that play a key role in the valve closing dynamics were also calculated over the closing phase: (1) the average closing trans-valvular pressure (DP), and (2) the reverse closing volume (RV). Both parameters contribute to the valve closing energy, E, in Joules (J). E was calculated from DP and RV as follows:

$$E = DP \times RV \quad (4)$$

The closing energy corresponds to the fluid energy that is involved in the valve closing process. Closing energy is the sum of the fluid viscous energy loss during valve closing and the work done in the mechanical deformation of both stent and leaflets during closing. It is not possible to separately quantify how much energy is dedicated to the deformation and how much is dedicated to the reverse flow. However, discussing the way DP and RV control the energy and interact together over the valve closing process helps to better understand the leaflet-stent interaction. Basically, from a fluid mechanics point of view, reverse volume generates pressure release, and the more limited that volume is, the higher the pressure is expected to be. However, in case the valve system is more flexible, for a given reverse volume the pressure is expected to be less important as the deformation of the system absorbs part of it. Moreover, when considering textiles in particular, the level of reverse flow can provide information about how the porosity of the fibrous construction evolves during closing. Thus, by studying these parameters it is possible to globally compare the deformability of valve designs.

Particle Image Velocimetry (PIV)

For PIV, the flow was seeded with fluorescent PMMA-Rhodamine B particles with diameters ranging from 1 to 20 μm. For all cases, the velocity field within the distal flow region was measured using high spatial and temporal resolution PIV. Briefly, this involved illuminating the flow region using a laser sheet created by pulsed Nd:YLF single cavity diode pumped solid state laser coupled with external spherical and cylindrical lenses while acquiring high-speed images of the fluorescent particles within the region. Time-resolved PIV images were acquired with a resulting spatial and temporal resolutions of 0.0380mm/ pixel and 500Hz respectively. Phase locked measurements were recorded for 4 phases of the cardiac cycle (acceleration, peak, deceleration and diastole) repetitively 250 times with a spatial resolution of 0.0380mm/pixel. Refraction was corrected using a calibration in DaVis

particle image velocimetry software (DaVis 7.2, LaVision Germany). Velocity vectors were calculated using adaptive cross-correlation algorithms. Further details of PIV measurements can be found in Hatoum et al[11, 13–15].

Vorticity Dynamics

Using the velocity measurements from PIV, vorticity dynamics were also evaluated distal to the valve. Vorticity is the curl of the velocity field and therefore captures rotational components of the blood flow shearing as well as visualizing turbulent eddies. Regions of high vorticity along the axis perpendicular to the plane indicate both shear and rotation of the fluid particles. Vorticity was computed using the following equation:

$$\omega_z = -(\frac{dV_x}{dy} - \frac{dV_y}{dx}) \quad (5)$$

Where ω_z is the vorticity component with units of s^{-1}; V_x and V_y are the x and y components of the velocity vector with units of m/s. The x and y directions are axial and lateral respectively with the z direction being out-of-measurement plane.

Reynolds shear stress (RSS)

Reynolds shear stress has been widely correlated to turbulence and platelet activation[6, 26]. It is a statistical quantity that measures the shear stress between fluid layers when fluid particles decelerate or accelerate while changing direction[8].

$$RSS = \rho\sqrt{\left(\frac{\overline{u'u'} - \overline{v'v'}}{2}\right)^2 + \left(\overline{u'v'}\right)^2} \quad (6)$$

Where ρ is the blood density and u' and v' are the instantaneous velocity fluctuations in the x and y directions respectively.

Statistics

All data are presented as mean ± standard deviation. Student t test was used to compare the means and $p < 0.05$ was considered statistically significant. Analyses were performed over 100 replicates.

Results

Hemodynamics

PG and LF are plotted in Fig. 3. PGs were found to be 11.86±0.51, 8.84±0.40, 11.59±0.12 and 7.05±0.09mmHg for RS-DB, RS-DT TAV, RS-RT TAV and DS-RT TAVs respectively. RS-DB PG was found to be the highest compared to the others with significant differences (p<0.01) except for RS-DB PG compared the RS-RT TAV (p=0.3). LFs were found to be 11.70±0.34, 29.80±0.76, 14.23±1.64 and 12.08±0.45% for RS-DB, RS-DT TAV, RS-RT TAV and DS-RT TAVs respectively. RS-DB LF was found to be the smallest without any

significant difference with the RS-RT TAV (p=0.065) and the DS-RT TAV (p=0.25) while compared with the other TAVs the differences were significant (p<0.01).

Leaflet kinematics

Fig. 4 shows snapshots of the *en-face* imaging of the TAVs at different phases in the cardiac cycle. **Video 1** also shows the TAVs imaging. The DS-RT TAV shows the most symmetric opening at peak followed by the RS-DT TAV, then the RS-RT TAV and lastly the RS-DB. The closing kinematics are evaluated quantitatively using the pinwheeling index (PI). PIs are shown in Figure 3. PIs were calculated to be 15.79±2.34%, 4.36±0.84%, 2.47±0.51% and 2.03±0.33% for RS-DB, RS-DT TAV, RS-RT TAV and DS-RT TAVs respectively and in descending order of magnitude. The only difference in PI that wasn't significant was found between the DS-RT TAV and the RS-RT TAV (p=0.23) while all the others were significant.

Valve closing dynamics

Results in Figure 5 bring out that the closing energy is the lowest for the braided DS-RT (0.0010±0.0002J), followed by RS-RT (0.0017±0.0002J), RS-DB (0.0023±0.0004J respectively) and the highest closing energy was found with the RS-DT TAV (0.0036±0.0007J). Compared to other valve cases, this case (DS-RT) yields the lowest closing volume (0.11±0.014 L over one closing cycle) followed by RS-RT and the RS-DB (0.23±0.040 and 0.23±0.026L respectively) and the highest closing volume was found with the RS-DT TAV (0.32±0.027L).

Flow velocity field and vorticity dynamics

Fig. 6 shows the phase averaged velocity vectors and vorticity contours at different phases in the cardiac cycle for the four different TAVs. During acceleration, RS-DB showed the highest velocity 1.753±0.007m/s followed by the RS-RT TAV 1.717±0.051m/s, then the RS-DT TAV 1.696±0.019m/s and the lowest velocity was obtained with the DS-RT TAV valve 1.43±0.023m/s. During peak systole, the highest velocity was obtained with the RS-RT TAV 2.374±0.095m/s, followed by the DS-RT TAV 2.119±0.032m/s, then the RS-DB 2.058±0.131m/s and the lowest velocity was obtained with the RS-DT TAV 2.022±0.05m/s. The differences between the RS-DT TAV velocity and the RS-DB velocity from one side and the DS-RT TAV velocity from another was found not significant (p=0.06 and p=0.32 respectively). The RS-RT TAV presented the highest velocity with significant differences with all the other TAVs (p<0.01). During deceleration, the highest velocity was obtained with the RS-DB 0.894±0.062m/s, followed by the RS-RT TAV 0.852±0.057m/s then the DS-RT TAV 0.732±0.06m/s and the lowest velocity was obtained with the RS-DT TAV 0.618±0.038m/s. During diastole for the 4 cases, the velocity was near zero ~0.088m/s. At peak systole where vorticity is highest, the highest vorticity was obtained with the RS-RT TAV 1039.6±9.099s^{-1} followed by the DS-RT TAV 831.2±7.694s^{-1}, then RS-DT TAV 762±9.381s^{-1} and the lowest was obtained with the RS-DB 745±9.083 s^{-1}. The jet direction with the RS-DB is oriented downwards and that of the DS-RT TAV is oriented upwards making the shear layers inclined in the same direction. Less diffusion is observed with the RS-DB compared to the other TAVs and very quick diffusion of the upper counterclockwise shear layer occurs with the DS-RT TAV.

Reynolds shear stress (RSS) fields

Fig. 7 shows the principal Reynolds shear stresses at different phases in the cardiac cycle for the different valves and models. The contour plots of the RSS mirror those of the vortical shear layer structures in Fig. 5 with RSS peaking in areas with more diffused shear layer vorticity. At peak systole where RSS values are highest, the lowest RSS was obtained with the RS-DT TAV 87.82±0.58Pa, then the RS-DB 108.42±1.47Pa, then the RS-RT TAV 117.8±3.7Pa and the highest was obtained with the DS-RT TAV 122.98±1.87Pa with the DS-RT TAV and the RS-RT TAV showing insignificant differences (p=0.1) while the rest showed significant differences (p<0.05). Deceleration is an interesting phase where adverse pressure gradient causes more turbulence. The lowest deceleration RSS is obtained with RS-DT TAV 40.11±0.55Pa followed by DS-RT 54.17±0.61Pa then RS-DB 60.83±0.5Pa and the maximum was found with RS-RT 67±0.17Pa (p<0.01).

Discussion

In this study, the differences occurring in the flow of the four different TAVs were assessed through evaluating (a) hemodynamic parameters, (b) leaflet kinematics, (c) deformation mechanics of the valve system and (d) turbulence. These differences are related to the leaflet-stent dynamics related to the deformability of the leaflet and/or stent.

Hemodynamics

The textile valves in general induce larger LFs than the biological control valve, as the material is porous consistent with previous literature[36]. However, the DS-RT valve presents the most optimal combination of PGs and LFs compared to the other valves highlighting the superiority of the stent, in particular when it is compared to the RS-RT.

Comparing DS-RT to RS-RT, the fabric used being the same in both devices (RT), it is the larger flexibility of the braided stent that improves the forward and reverse performance. During the opening phase, the stent can slightly deform radially towards enlargement, thus limiting the flow obstruction (PG=7.05mmHg vs. 11.59mmHg). Conversely, during closing, the stent deforms radially inwards which promotes leaflet coaptation.

While yielding lower PG, the material of the RS-DT compared to RS-RT led to 2 times higher LF (29.8 % vs 14.23 %). In fact, the fabric obtained from diagonally oriented yarns (RS-DT) is much more deformable than the material of the RS-RT. When submitted to reverse pressure, the textile deforms. Yarns involved in the construction, which are initially in a crimped configuration, become stretched. With the yarn density remaining constant over the leaflet surface area, pores in the fabric tend to open and the leakage increases. Conversely, the limited deformation undergone by yarns in the RS-RT limits the porosity increase and consequently lesser leakage.

Comparing RS-DB with RS-RT, it seems that the different leaflet materials behave differently especially when it comes to leaflet deformation over the closing process and overall deformability of the stent valve system which are described below in more details. The biological tissue being less porous than the textile one provides better sealing which explains the lower leakage fractions.

Future studies are needed with a DS-DB valve for a broader understanding of hemodynamics.

Leaflet kinematics

PI is a dimensionless index used to quantify valve leaflet deformation severity (wrinkling) and coaptation mismatch. All the valves specifically transcatheter ones pinwheel and high PIs are often associated with low durability therefore accelerated failure of bioprosthetic valve leaflets[5, 9, 23]. One reason of pinwheeling is the high stresses developed on the leaflets as demonstrated by Li et al[20] and Maleki et al[22]. RS-DB showed significantly higher pinwheeling indices than the other models highlighting the superiority of the textile materials whether rigid or deformable compared to the bioprosthetic ones. Consequently, more folds are induced in the RS-DB in diastole compared to the other devices as can be seen in Figure 4 and as shown in previous studies[16]. This makes the biological leaflets more prone to deterioration than the textile ones.

Pinwheeling decreases further with a deformable stent compared to a rigid one confirming the influence of the stent radial inwards deformation in providing better leaflet positioning during closing time and better coaptation. Studies have been performed highlighting that pinwheeling effect was neglected or removed due to the relief of strains caused by flexion of the stent post specifically at the commissure posts[9]. This reinforces the idea that the interaction between the rigid stent and the deformable leaflet seems to be optimal when it comes to pinwheeling and thus durability.

Valve closing dynamics

The elastic deformability assessment during valve closure provides information on how compliant the constituents as a system (stent and leaflets) of the valves are during closing mechanism. Two main observations can be made from the results presented in Figure 5. First, the braided DS-RT yielded the lowest closing energy (0.001 J) in particular compared to RS-RT (0.0017 J), designed with the same fabric but with a more rigid stent. Most of the energy yielded in that latter case, corresponds to the leakage across the device, as the closing volume was twice as large for RS-RT (0.23 vs 0.11). The limited closing volume for DS-RT would have supposed only limited pressure release, but the pressure was actually only 20 % larger (4.31% vs 3.44%) in that case. This suggests that the valve system is deformable enough to partially damp the closing forces and the reverse pressure. The straight (rigid) textile used - being not very elastic - one can assume that the elasticity is provided by the stent in that case. The system is even slightly more flexible than the RS-DB control system for which both the pressure and the leakage volume are more important. This confirms that the more elastic stent seems to provide an advantage in terms of elastic deformability of the valve system.

Second, when comparing the inclined (deformable) textile with the straight (rigid) one, both assembled on the rigid stent, it appears that the leakage volume is 40% higher for the inclined material (0.32 vs 0.23) whereas the closing energy is almost twice as large (0.0036 vs 0.0017J). In that case, one can assume that a large part of that energy is dissipated into fabric deformation. As already mentioned previously, the textile construction designed with

inclined yarns (RS-DT) is highly deformable under reverse pressure compared to the straight yarn design (RS-RT) despite the stent design and the textile surface area are the same in both devices. In that configuration, one can assume that the energy involved in the fabric deformation would help damping the forces directly applied on the valve-stent fixation.

Flow velocity field and vorticity dynamics

The flow velocity fields and shear layers are different among the different valves and this can be due to different design and material properties. Despite having statistically significant differences at peak systole where velocities are highest among some of the different cases, but from a clinical standpoint the velocities all fall within the same range and order. The flow across these TAVs is turbulent by nature and turbulence is characterized by high levels of fluctuating vorticity. For this reason, vorticity dynamics play an essential role in the description of turbulent flows[19]. This explains the high levels of fluctuating vorticity as is evident in Fig. 6 contours for all the 4 TAVs. Relating the opening imaging dynamics to the orientation of the shear layers, during acceleration for the RS-DB, the leaflet at the left was not fully open and the shear layers were not pointing downwards during acceleration in Fig. 6. Then at peak when all leaflets were open, the orientation moved downwards. Having the leaflet at the left the last to open and a downward jet may be related to a higher resistance to flow provided by the leaflet especially that its fully open configuration at peak from Fig. 4 shows a twist. Regarding the upward oriented jet in the DS-RT TAV and also relating the opening imaging dynamics to the orientation of the shear layers, the bottom leaflet occupies around 50% of the circular valve area making it harder for the flow to maintain it fully open at all times thus generating an upward oriented jet.

Reynolds shear stress (RSS) fields

The importance of RSS arises from its connection to platelet activation and its account of the turbulent fluctuations of the blood velocity[6, 10, 16, 17, 26, 31]. Reynolds stress is produced when fluid particles decelerate or accelerate while changing direction[17]. The onset of platelet activation ranges 10 to 100 Pa[3]. It seems that all TAVs - except the RS-DT TAV - cross the upper threshold of 100Pa defined as the onset of platelet activation[3, 21, 28] with the RS-DB yielding an intermediate value. The RS-DB's peak values come in accordance with those found in a similar study by Gunning et al[8]. Turbulence studies have emphasized the effect of porous media on increasing the flow turbulence, unsteadiness and chaos[1, 25]. This may provide a possible explanation to the reason why textiles yielded high RSS values. In addition, and combining results from the previous sections, the textile deformation can also increase friction between yarns, which could accelerate the inter-surface drag enhancing RSS. An in-vitro study by Doreen et al highlighted the impact of the RS-DB structure on enhancing platelet activation thus thrombus formation[29]. Ultimately, given that most TAV types exceed 100Pa, TAV associated risk of leaflet thrombosis or thrombosis in general is dependent on many factors besides RSS, mainly sinus washout[12, 15]. Having said that, in deceleration, RSS values highlight the importance and advantage of the DS-RT stent when compared to RS-RT. Both peak and deceleration phases emphasize the advantage that RS-DT leaflet material has on minimizing turbulent stresses however not significantly to mitigate platelet activation.

Conclusion

The hemodynamic performance, compliance and turbulence of three 19mm textile TAVs with different stents and textile material (RS-DT, RS-RT and DS-RT) were compared in this study with a control case involving a bioprosthetic TAV with the same stent as 2 of the 3 textile valves (RS-DB). From hemodynamic data and energy analysis, a combination of deformable stent and rigid textile (DS-RT) yielded an optimal performance and may potentially lead the next generation of textile heart valve design. Despite achieving more RSS than the rest of the TAVs, DS-RT still falls within the same range of RSS produced by any other transcatheter aortic valve whether textile or biological. Further in-vivo studies are needed to validate the in-vitro results.

Acknowledgments

References

1. Antohe BV, Lage JL. A General Two-Equation Macroscopic Turbulence Model for Incompressible Flow in Porous Media. International Journal of Heat and Mass Transfer. 1997; 40:3013–24.

2. Dasi Lakshmi P, Hatoum HodaKheradvar ArashZareian RaminAlavi S HamedSun WeiMartin CaitlinPham ThuyWang QianMidha Prem A. On the Mechanics of Transcatheter Aortic Valve Replacement. Annals of biomedical engineering. 2017; 45:310–31. [PubMed: 27873034]

3. Dasi Lakshmi P, Simon Helene A, Sucosky PhilippeYoganathan Ajit P. Fluid Mechanics of Artificial Heart Valves. Clinical and experimental pharmacology and physiology. 2009; 36:225–37. [PubMed: 19220329]

4. Dasi Lakshmi PrasadMorshed Khandakar NiazForleo Marcio. Phenomenology of Hemolysis in Turbulent Flows. ASME 2013 Summer Bioengineering Conference; American Society of Mechanical Engineers; 2013. V01AT05A020–V01AT05A20.

5. Doose ChristianKütting MaximilianEgron SandrineGhalati Pejman FarhadiSchmitz ChristophUtzenrath MarcSedaghat AlexanderFujita BuntaroSchmitz-Rode ThomasEnsminger Stephan. Valve-in-Valve Outcome: Design Impact of a Pre-Existing Bioprosthesis on the Hydrodynamics of an Edwards Sapien Xt Valve. European Journal of Cardio-Thoracic Surgery. 2016:ezw317.

6. Giersiepen M, Wurzinger LJ, Opitz R, Reul H. Estimation of Shear Stress-Related Blood Damage in Heart Valve Prostheses--in Vitro Comparison of 25 Aortic Valves. The International journal of artificial organs. 1990; 13:300–06. [PubMed: 2365485]

7. Giersiepen M, Wurzinger LJ, Opitz R, Reul H. Estimation of Shear Stress-Related Blood Damage in Heart Valve Prostheses-in Vitro Comparison of 25 Aortic Valves. The International journal of artificial organs. 1990; 13:300–06. [PubMed: 2365485]

8. Gunning Paul S, Saikrishnan NeelakantanMcNamara Laoise M, Yoganathan Ajit P. An in Vitro Evaluation of the Impact of Eccentric Deployment on Transcatheter Aortic Valve Hemodynamics. Annals of biomedical engineering. 2014; 42:1195–206. [PubMed: 24719050]

9. Gunning Paul S, Saikrishnan NeelakantanYoganathan Ajit P, McNamara Laoise M. Total Ellipse of the Heart Valve: The Impact of Eccentric Stent Distortion on the Regional Dynamic Deformation of Pericardial Tissue Leaflets of a Transcatheter Aortic Valve Replacement. Journal of The Royal Society Interface. 2015; 12:20150737.

10. Hanle DD, Harrison EC, Yoganathan AP, Corcoran WH. Turbulence Downstream from the Ionescu-Shiley Bioprosthesis in Steady and Pulsatile Flow. Medical and Biological Engineering and Computing. 1987; 25:645–49. [PubMed: 3505303]

11. Hatoum HodaDollery JenniferLilly Scott M, Crestanello Juan A, Dasi Lakshmi Prasad. Effect of Severe Bioprosthetic Valve Tissue Ingrowth and Inflow Calcification on Valve-in-Valve Performance. Journal of biomechanics. 2018; 74:171–79. [PubMed: 29753455]

12. Hoda HatoumJennifer DolleryScott LillyJuan CrestanelloPrasad Dasi Lakshmi. Implantation Depth and Rotational Orientation Effect on Valve-in-Valve Hemodynamics and Sinus Flow. The Annals of thoracic surgery. 2018

13. Hatoum HodaDollery JenniferLilly Scott M, Crestanello JuanDasi Lakshmi Prasad. Impact of Patient Morphologies on Sinus Flow Stasis in Transcatheter Aortic Valve Replacement: An in-Vitro Study. The Journal of Thoracic and Cardiovascular Surgery. 2018

14. Hatoum HodaDollery JenniferLilly Scott M, Crestanello Juan A, Dasi Lakshmi Prasad. Implantation Depth and Rotational Orientation Effect on Valve-in-Valve Hemodynamics and Sinus Flow. The Annals of Thoracic Surgery.

15. Hatoum HodaMoore Brandon L, Maureira PabloDollery JenniferCrestanello Juan A, Dasi Lakshmi Prasad. Aortic Sinus Flow Stasis Likely in Valve-in-Valve Transcatheter Aortic Valve Implantation. The Journal of Thoracic and Cardiovascular Surgery.

16. Hatoum HodaYousefi AtiehLilly ScottMaureira PabloCrestanello JuanDasi Lakshmi P. An in-Vitro Evaluation of Turbulence after Transcatheter Aortic Valve Implantation. The Journal of Thoracic and Cardiovascular Surgery. 2018

17. Jones Steven A. A Relationship between Reynolds Stresses and Viscous Dissipation: Implications to Red Cell Damage. Annals of biomedical engineering. 1995; 23:21–28. [PubMed: 7762879]

18. Khoffi FouedHeim FredericChakfe NabilLee Jason T. Transcatheter Fiber Heart Valve: Effect of Crimping on Material Performances. Journal of Biomedical Materials Research Part B: Applied Biomaterials. 2015; 103:1488–97.

19. Laufer John. New Trends in Experimental Turbulence Research. Annual Review of Fluid Mechanics. 1975; 7:307–26.

20. Li KeweiSun Wei. Simulated Transcatheter Aortic Valve Deformation: A Parametric Study on the Impact of Leaflet Geometry on Valve Peak Stress. International journal for numerical methods in biomedical engineering. 2017; 33

21. Liu JS, Lu PC, Chu SH. Turbulence Characteristics Downstream of Bileaflet Aortic Valve Prostheses. Journal of biomechanical engineering. 2000; 122:118–24. [PubMed: 10834151]

22. Maleki HodaShahriari ShahrokhLabrosse MichelRodés-Cabau JosepPibarot PhilippeKadem Lyes. Effect of Aortic Annulus Size and Prosthesis Oversizing on the Hemodynamics and Leaflet Bending Stress of Transcatheter Valves: An *in Vitro* Study. Canadian Journal of Cardiology. 2015; 31:1041–46. [PubMed: 26211709]

23. Martin CaitlinSun Wei. Simulation of Long-Term Fatigue Damage in Bioprosthetic Heart Valves: Effects of Leaflet and Stent Elastic Properties. Biomechanics and modeling in mechanobiology. 2014; 13:759–70. [PubMed: 24092257]

24. Morshed Khandakar NiazBark David, JrForleo MarcioDasi Lakshmi Prasad. Theory to Predict Shear Stress on Cells in Turbulent Blood Flow. PloS one. 2014; 9:e105357. [PubMed: 25171175]

25. Mößner M, Radespiel R. Flow Simulations over Porous Media–Comparisons with Experiments. Computers & Fluids. 2017; 154:358–70.

26. Nygaard H, Giersiepen M, Hasenkam JM, Reul H, Paulsen PK, Rovsing PE, Westphal D. Two-Dimensional Color-Mapping of Turbulent Shear Stress Distribution Downstream of Two Aortic Bioprosthetic Valves in Vitro. Journal of biomechanics. 1992; 25:437–40.

27. Padala MuralidharSarin Eric L, Willis PatrickBabaliaros VasilisBlock PeterGuyton Robert A, Thourani Vinod H. An Engineering Review of Transcatheter Aortic Valve Technologies. Cardiovascular Engineering and Technology. 2010; 1:77–87.

28. Ramstack JM, Zuckerman L, Mockros LF. Shear-Induced Activation of Platelets. Journal of biomechanics. 1979; 12:113–25. [PubMed: 422576]

29. Richardt DoreenHaban-Rackebrandt Sherazade LuiseStock SinaScharfschwerdt MichaelSievers Hans-Hinrich. A Matter of Thrombosis: Different Thrombus-Like Formations in Balloon-Expandable Transcatheter Aortic Valve Prostheses. European Journal of Cardio-Thoracic Surgery. 2018

30. Rodés-Cabau Josep. Transcatheter Aortic Valve Implantation: Current and Future Approaches. Nature Reviews Cardiology. 2012; 9:15.

31. Schoephoerster Richard T, Chandran Krishnan B. Velocity and Turbulence Measurements Past Mitrial Valve Prostheses in a Model Left Ventricle. Journal of biomechanics. 1991; 24:549–62. [PubMed: 1880139]

32. Singhal PoojaLuk AdrianaButany Jagdish. Bioprosthetic Heart Valves: Impact of Implantation on Biomaterials. ISRN Biomaterials. 2013; 2013

33. Vaesken AntoineHeim FredericChakfe Nabil. Fiber Heart Valve Prosthesis: Influence of the Fabric Construction Parameters on the Valve Fatigue Performances. Journal of the mechanical behavior of biomedical materials. 2014; 40:69–74. [PubMed: 25201184]

34. Vaesken AntoinePelle AnnePavon-Djavid GracielaRancic JeanneChakfe NabilHeim Frederic. Heart Valves from Polyester Fibers: A Preliminary 6-Month in Vivo Study. Biomedical Engineering/Biomedizinische Technik. 2017

35. Yoganathan Ajit P, Chandran KB, Sotiropoulos Fotis. Flow in Prosthetic Heart Valves: State-of-the-Art and Future Directions. Annals of biomedical engineering. 2005; 33:1689–94. [PubMed: 16389514]

36. Yousefi AtiehVaesken AntoineAmri AmnaDasi Lakshmi PrasadHeim Frederic. Heart Valves from Polyester Fibers Vs. Biological Tissue: Comparative Study in Vitro. Annals of biomedical engineering. 2017; 45:476–86. [PubMed: 27150672]

37. Yun B MinDasi LP, Aidun CK, Yoganathan AP. Highly Resolved Pulsatile Flows through Prosthetic Heart Valves Using the Entropic Lattice-Boltzmann Method. Journal of Fluid Mechanics. 2014; 754:122–60.

Highlights

- The textile valves in general induce larger leakage fractions than the biological valve, as the material is porous.

- Having a deformable stent with rigid leaflets in a valve presents the combination of the lowest transvalvular pressure gradients and leakage fractions compared to the other textile valves highlighting the superiority of the stent, in particular when it is compared to the rigid stent rigid leaflet combination. The fabric used being the same in both devices, it is the larger flexibility of the braided stent which improves the forward and reverse performance.

- Biological leaflet material and rigid textile materials behave differently especially when it comes to leaflet deformation over the closing process and overall deformability of the stent valve system which are described below in more details.

- Rigid stent biological leaflet valve showed significantly higher pinwheeling indices than the other models highlighting the superiority of the textile materials to the biological ones.

- The more elastic stent seems to provide an advantage in terms of elastic deformability of the valve system.

- The energy involved in the fabric deformation would help damping the forces directly applied on the valve-stent fixation.

- Reynolds shear stress values at peak systole fall within the same range irrespective of the valve nature.
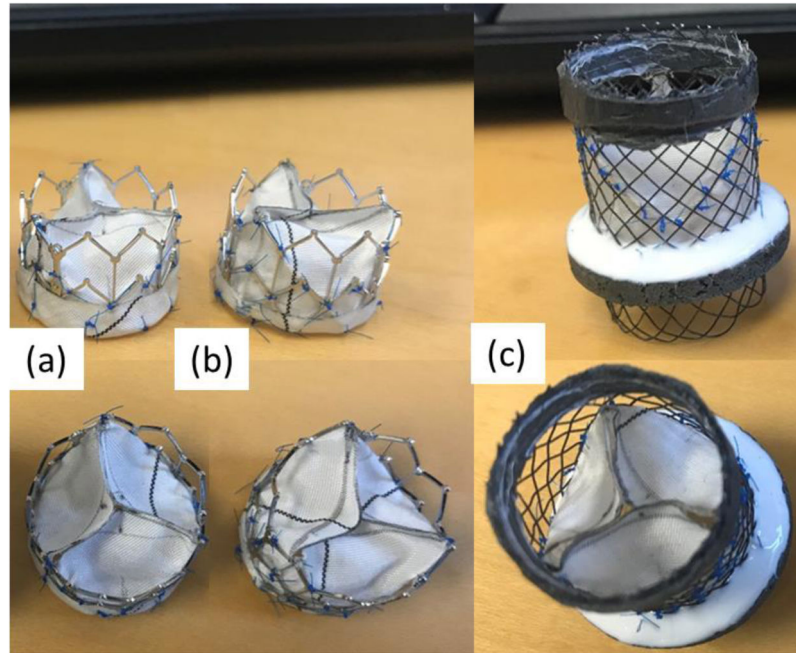
Figure 1.
(a) Rigid stent with deformable textile (RS-DT), (b) rigid stent with straight textile (RS-RT) and (c) Deformable stent with straight textile (DS-RT) TAVs.
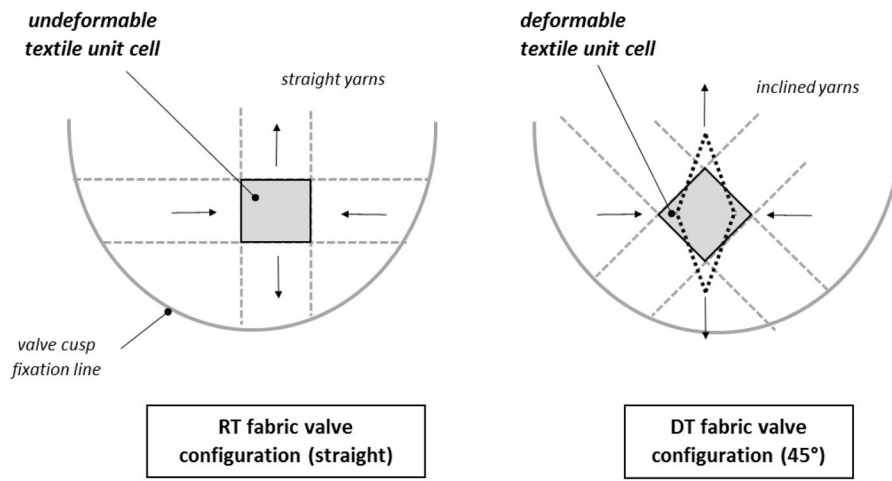
Figure 2.
Schematic diagram showing the difference in textile material behavior between RT and DT.
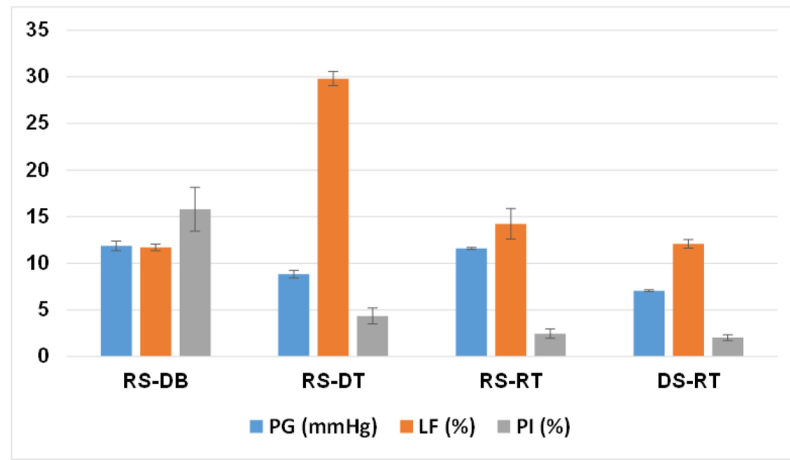
Figure 3.
Key hemodynamic parameters (transvalvular pressure gradients, leakage fractions and pinwheeling) of the 4 valves averaged over 100 cycles. Values are reported as mean ± standard deviation.
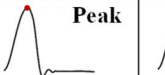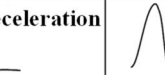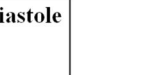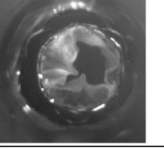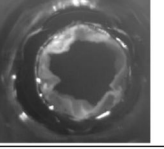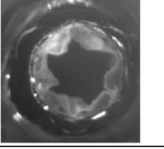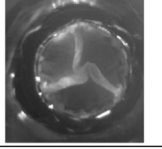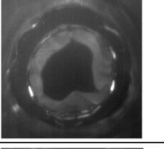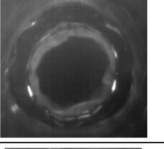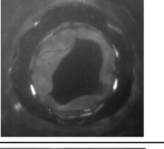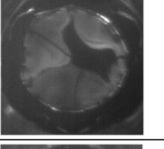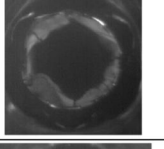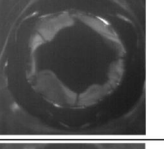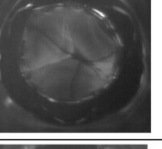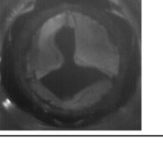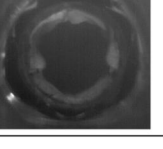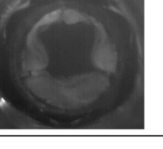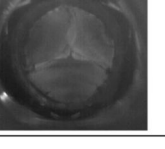
Figure 4.
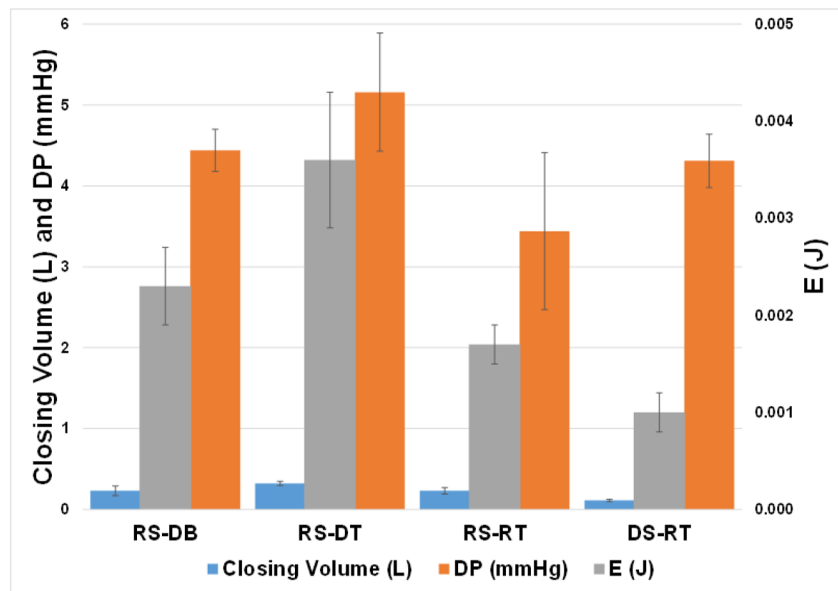En-face imaging of the valves at different phases in the cardiac cycle.

Figure 5.
Closing volume, closing pressure gradient and closing energy values per cardiac cycle of the 4 valves averaged over 100 cycles. Values are reported as mean ± standard deviation.
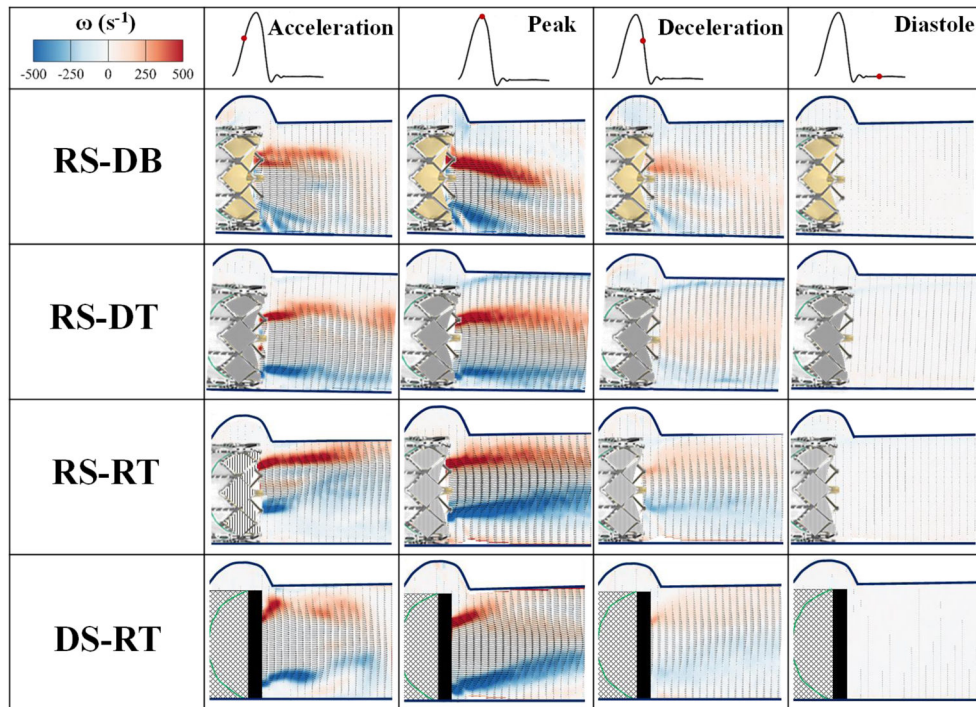
Figure 6.
Phase averaged velocity vectors and vorticity contours at different phases in the cardiac cycle for the four different valves.
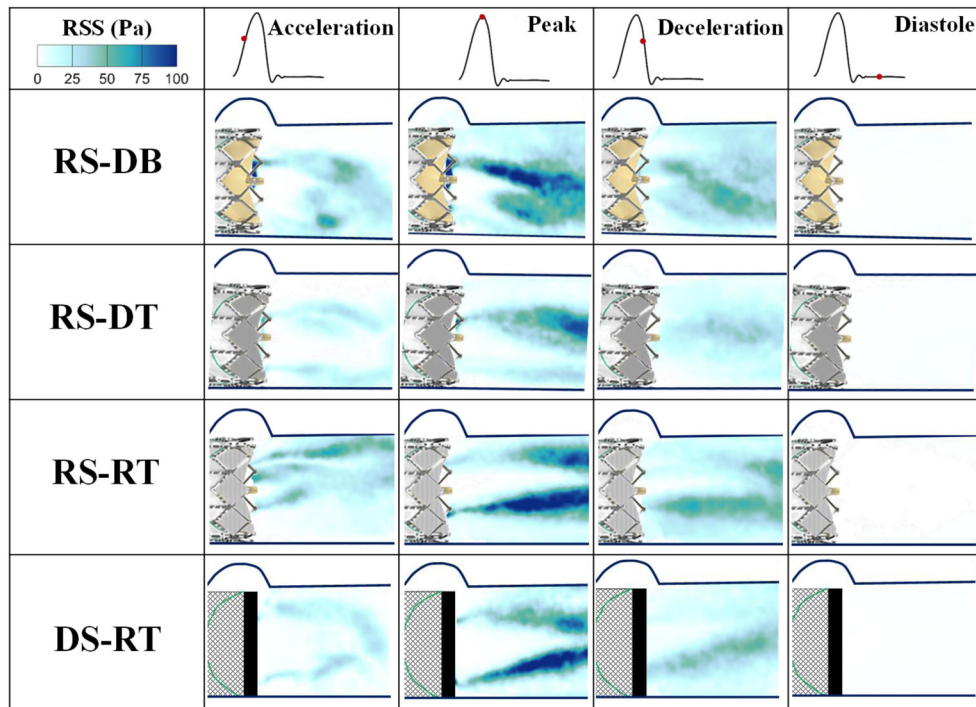
Figure 7.
Principal Reynolds shear stresses at different phases in the cardiac cycle.

Table 1

Textile RT and DT material properties. DT is formed of the same material as RT only oriented differently (45°) relatively to the stent axis.

TEXTILE MEMBRANE	
Yarn structure	Multifilament
Thickness(μm for 0.5 gf/cm^2)	183
Porosity (%)	71
Permeability (ml/cm^2/s)	790
Roughness SMD (μm)	17.7
Surface density (g/m^2)	74
Yarn density, warp (yarns/cm)	75
Yarn density, weft (yarns/cm)	50
Filament diameter (μm)	10
Yarn count (tex)	5.45